The Meteoritical Society

Meteoritics & Planetary Science 55, Nr 11, 2360–2374 (2020)
doi: 10.1111/maps.13590

Quartz and cristobalite ballen in impact melt rocks from the Ries impact structure, Germany, formed by dehydration of shock-generated amorphous phases

Claudia A. TREPMANN[1*], Fabian DELLEFANT[1], Melanie KALIWODA[2], Kai-Uwe HESS[1], Wolfgang W. SCHMAHL[1,2], and Stefan HÖLZL[3]

[1]Department of Earth and Environmental Sciences, Ludwig-Maximilians-University, 80333 Munich, Germany
[2]Mineralogische Staatssammlung, Staatliche naturwissenschaftliche Sammlungen Bayerns, 80333 Munich, Germany
[3]RiesKraterMuseum, Staatliche naturwissenschaftliche Sammlungen Bayerns, 86720 Nördlingen, Germany
[*]Corresponding author. E-mail: claudia.trepmann@lmu.de

(Received 19 March 2020; revision accepted 06 October 2020)

Abstract–Quartz and cristobalite ballen aggregates surrounded by dendritic cristobalite in gneiss clasts of impact melt rocks from the Ries impact structure are analyzed by Raman spectroscopy, microscopy, and electron backscattered diffraction to elucidate the development of the characteristic polycrystalline ballen that are defined by curved interfaces between each other. We suggest that the investigated ballen aggregates represent former fluid inclusion-rich quartz grains from the granitic gneiss protolith. Upon shock loading, they transformed into an amorphous phase that partly retained information on the precursor structure. Volatiles from inclusions dissolved into the amorphous phase. During decompression and cooling, dehydration takes place and causes fracturing of the amorphous phase and disintegration into small globular ballen, with the fluid being expelled along the fractures. A similar formation of small globules due to dehydration of silica-rich glass is known for perlitic structures of volcanic rocks. Remnants of the precursor structure are present in the amorphous phase and enabled topotactic crystallization of quartz, leading to a crystallographic preferred orientation. Crystallization of more distorted parts of the amorphous phase led to random orientations of the quartz crystals. Ballen comprised of cristobalite formed from a dehydrated amorphous phase with no structural memory of the precursor. Dendritic cristobalite exclusively occurring at the rim of quartz ballen aggregate is interpreted to have crystallized directly from a melt enriched in fluids that were expelled during dehydration of the amorphous phase.

INTRODUCTION

"Ballen" of quartz and cristobalite aggregates have been observed in impactites from a number of terrestrial impact structures, predominantly from impact melt rocks, suevites, and target rock clasts affected by high post-shock temperatures ($T \geq 1200$ °C, e.g., Short 1970; Engelhardt 1972; Carstens 1975; Bischoff and Stöffler 1984; Rehfeldt-Oskierski et al. 1986; French 1998; Osinski 2004; Ferrière et al. 2008, 2009, 2010; Buchner et al. 2010; Chen et al. 2010; Schmieder et al. 2014; Chanou et al. 2015). The ballen are characterized by aggregates of globular quartz and/or cristobalite that can in rare cases contain small inclusions of coesite (Ferrière et al. 2010). Based on polarized light microscopy, Bischoff and Stöffler (1984) distinguished three types of ballen, which they interpreted to crystallize at various shock pressures from an impact-generated diaplectic glass that can preserve the shape of the original quartz grain and retains remnants of the original crystalline structure. Type A (~30–35 GPa) is described as optically homogeneous, type B (~45–55 GPa) shows variable crystallographic orientations, and type C (>50 GPa) is described as newly crystallized from a melt. Ferrière et al. (2008, 2009) distinguished five different types: Type I is defined as α-cristobalite ballen with homogeneous extinction, types II–V as α-quartz ballen with either homogeneous extinction (type

II), heterogeneous extinction (type III), intraballen crystallization (type IV), or chert-like ballen (type V). Ferrière et al. (2009) concluded that the ballen aggregates are the result of back-transformations from shock-induced states and different types of ballen do not indicate specific shock pressures, but that shock pressures in excess of ~35 GPa are required for all of them to form either from diaplectic glass or from a silica melt (lechatelierite). Furthermore, brownish colored, so-called "toasted" ballen have been reported (Whitehead et al. 2002; Ferrière et al. 2010). Various models for the formation of the ballen aggregates have been proposed to date, which mostly include multiple silica phase transformations (Short 1970; Engelhardt 1972; Carstens 1975; French 1998; Ferrière et al. 2009, 2010). Ferrière et al. (2010) suggested from a compilation of quartz and cristobalite ballen aggregates from different impact structures that α-quartz in ballen is the product of back-transformation of β-quartz and/or α-cristobalite with time.

Yet, the detailed formation mechanism of the ballen shape and especially the role of multiple phase transformations from quartz to amorphous phases back to cristobalite and/or quartz, as well as the conditions under which ballen form, remain unclear (Ferrière et al. 2010). The existing ballen classifications are based on the dominant phase comprising the ballen (quartz or cristobalite) and the optical extinction characteristics (Bischoff and Stöffler 1984; Ferrière et al. 2008, 2009). Optical extinction characteristics result from crystallographic misorientations, which can be analyzed and quantified by the electron backscatter diffraction (EBSD) technique. Using EBSD, we will describe this microfabric, including the crystallographic orientations of quartz and cristobalite in ballen aggregates within granitic gneiss clasts from the Polsingen impact melt rocks of the Ries impact structure, Germany, and we discuss the conditions and the formation mechanisms of ballen based on these observations. Although quartz ballen aggregates and dendritic rims of cristobalite around ballen aggregates are well known from the Ries (e.g., Engelhardt 1972; Ferrière et al. 2009, 2010; Osinski 2004), cristobalite ballen aggregates have, to our knowledge, not been described from the Ries impact structure so far.

METHODS

Impact melt rocks were sampled in April 2018 at the old quarry southwest of Polsingen, in the Ries impact structure, Germany (e.g., Stöffler et al. 2013). From five samples, polished thin sections (~30 μm) were prepared that were analyzed by polarized light microscopy. Two samples (CT915, CT917) were chosen for detailed scanning electron microscopy (SEM) and Raman spectroscopy.

EBSD allow us to measure the 3-D crystallographic orientation of crystalline material by SEM (scanning electron microscope) and to quantify misorientations within crystals and between different grains. For EBSD analyses, an additional chemo-mechanical polish with a colloidal silica solution (Syton) was applied. SEM investigations including EBSD and energy dispersive spectroscopy (EDS) were performed on the carbon-coated thin sections using a Hitachi SU5000 microscope, equipped with a field emission gun, NordlysNano high-sensitivity detector (Oxford Instruments), EDS detector (Oxford instruments), and MiniCL detector (Gatan). For EDS and EBSD data acquisition, the AZtec analysis software (Oxford Instruments) was used. The SEM was operated at accelerating voltages of 20 kV and a working distance of 10–25 mm. The step size for automatic EBSD mapping using a sample holder pre-tilted at 70° with respect to the electron beam was in the range of 0.5–2 μm, dependent on the EBSD pattern quality and required resolution. The EBSD data were processed using the Channel software (Oxford Instruments). All pole figures are stereographic projections of the lower hemisphere.

Silica displays abundant polymorphism as a function of temperature and pressure (e.g., Boyer et al. 1985; Stähle et al. 2008). Therefore, in situ Raman spectroscopic investigations were carried out to identify the SiO_2 phases present in a sample by using a HORIBA JOBIN YVON XploRa ONE micro Raman machine at the Mineralogical State Collection Munich (SNSB). This specific Raman spectrometer was equipped with edge filters, a Peltier-cooled CCD detector, and three different lasers working at 532 nm (green), 638 nm (red), and 785 nm (near IR). A green 2ω-Nd:YAG laser (532 nm) was used in an attenuated mode of 50% laser power belonging to 5.5 + 0.1 mW on the sample surface. Focusing was completed through a 100 LWD (long working distance) objective, resulting in a 0.9 μm laser spot size on the sample surface. The wavelength calibration of the green laser was performed by manual calibration with a pure Si wafer chip; the main peak was located in the interval of 520 ± 1 cm^{-1}. The wave number reproducibility was checked several times a day within deviations of less than <0.2 cm^{-1}. Monthly deviation was in the range of 1 cm^{-1} before calibration. Hole and slit were set to 300 and 100 μm. The 1200T/1800 T grating was used to obtain a better spectral resolution. Short counting times (2 × 8 s) were chosen. The precision of determining Raman peak positions by this method is estimated to be ±1 to ±1.5 cm^{-1}. In addition to single point measurements,

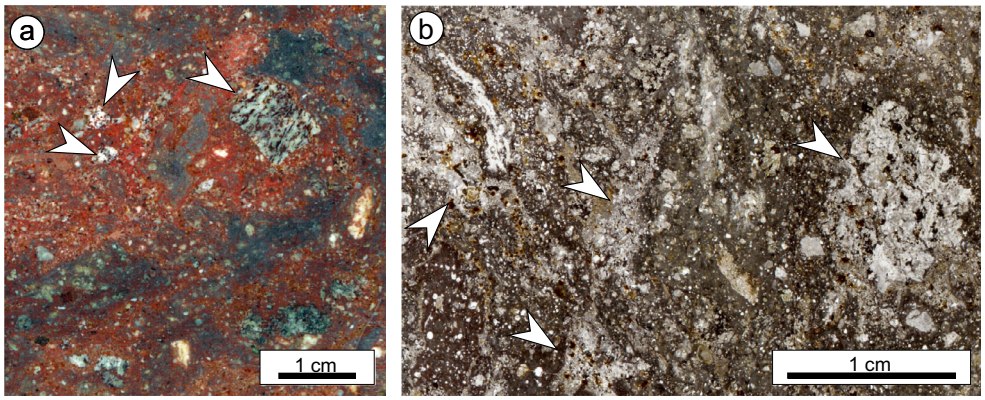

Fig. 1. Impact melt rock from Polsingen. a) Hand specimen and (b) thin section of sample CT917 showing a red matrix and clasts of granitic gneisses (arrows). (Color figure can be viewed at wileyonlinelibrary.com.)

several mapping efforts inside the quartz and cristobalite ballen have been performed to check the phase distributions.

SAMPLES

The studied ballen occur in impact melt rocks from the old quarry southwest of Polsingen within the 15 Ma old, 26 km diameter Ries impact structure, Germany (for a recent review of the Ries, see Stöffler et al. 2013). The outcrop is located about 11 km to the northeast of the assumed center of the crater, and is located in the megablock zone (N48°55′03″/E10°42′21″, Fig. 1), beyond the inner ring, the typical radial range for these rare, melt-rich deposits of the Ries (e.g., Engelhardt 1997; Buchner et al. 2010; Stöffler et al. 2013). These impact melt rocks are characterized by a large amount of biotite-bearing granitic gneiss fragments in a red melt matrix due to finely dispersed hematite (Fig. 1). In the granitic gneiss clasts, ballen aggregates, vesicles, and decomposed biotite are common (Figs. 2a and 2b). The composition of the Polsingen impact melt matrix has been reported to be similar to the impact melt rock drilled at Enkingen, as well as to the melt particles in the frequently occurring "outer suevites," containing about 6–9 wt% $Na_2O + K_2O$ and 60–65 wt% SiO_2 (Osinski 2004; Stöffler et al. 2013). This vesicle-rich impact melt rock from Polsingen with decomposed biotite indicates a shock stage F6 (former shock stage III), for granitic target rocks after Stöffler et al. (2018), representing a shock pressure range of 45–60 GPa and postshock temperatures of 900–1300 °C. The occurrence of these melt rocks at Polsingen most likely represents an erosional remnant of an originally more widespread impact melt sheet (e.g., Engelhardt and Graup 1984; Osinski 2004; Buchner et al. 2010; Stöffler et al. 2013).

RESULTS

The ballen aggregates comprised of individual ballen occur within the granitic gneiss clasts of the impact melt rocks (Fig. 2). They are mostly composed of pure α-quartz (Fig. 3A) and more rarely partly composed of α-cristobalite (Figs. 2f, 2g, and 3B). The spectra of α-quartz show the typical Raman peaks at 127, 205, 262, 354, 394, and 800 cm^{-1} as well as a main peak at 464 cm^{-1} (Fig. 3A). α-cristobalite in the ballen shows the typical triplet at 113, 231, and 418 cm^{-1} and a weaker peak at 785 cm^{-1} (Fig. 3B). A rim of brownish cristobalite is surrounding a ballen aggregate only where it is in contact with a vesicle in the impact melt rock (Figs. 2h and 3C).

The ballen aggregates have typically a diameter of a few hundreds of μm to 1 mm and show a rectangular (Fig. 2b) or an irregular shape (Figs. 2c and 2f–h). Partly, they can preserve the shape of the original quartz grain from the host rock (Fig. 2b) or they can exhibit the shape of a droplet (Fig. 2c). No structures indicating significant viscous flow within the aggregates are evident. The individual ballen are globules of a few tens of μm in diameter (Fig. 2). Quartz within individual ballen is characterized by undulatory extinction (Figs. 2c–f), which is also apparent as orientation contrast in BSE images (Figs. 4a and 4b). Cristobalite ballen show a radiating orientation contrast in BSE images (Fig. 4d). The curved interfaces defining the individual ballen can be open (Figs. 4a and 4b) or partly filled by siliceous material rich in Fe, K, Al, and Mg (Figs. 4c and 4d), as indicated by EDS measurements. Quartz that retains its original shape but with curved fractures forming incipient individual ballen can show several sets of planar features parallel to the basal plane (0001) and {10-13} rhombohedral planes, as indicated by EBSD measurements (Figs. 4e and 4f).

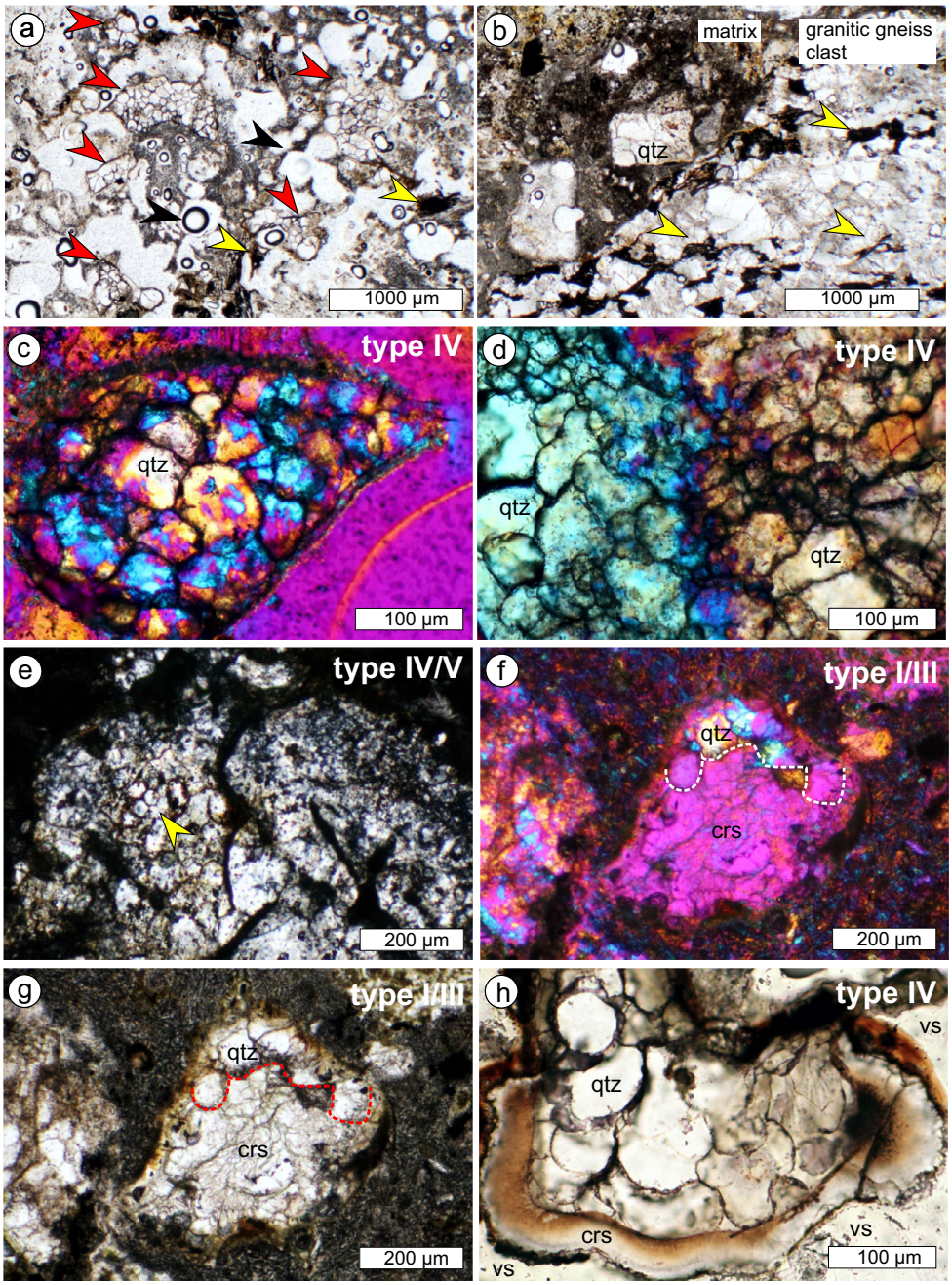

Fig. 2. Polarized light micrographs of ballen silica. a) Irregular aggregates of quartz with ballen (red arrows) in matrix rich in vesicles, sample CT915. Yellow arrows mark decomposed biotite. Black arrows point to vesicles. b) Quartz grain with preserved original shape and incipient ballen (qtz, type IV), sample CT917, compare Figs. 4e, 4f, and 9. Yellow arrows mark decomposed biotite in coarse-grained granitic gneiss clast component. c) Droplet-shaped quartz aggregate with ballen and heterogeneous extinction (type IV), crossed polarizers, and compensator plate inserted, sample CT915. d) Ballen showing two domains with slightly different crystallographic orientations and heterogeneous extinction of single ballen (type IV), crossed polarizers and compensator plate inserted, sample CT915. e) Ballen quartz with "chert-like" extinction (type V, where quartz ballen are hardly visible) but also areas displaying a heterogeneous extinction (type IV, ballen distinct, yellow arrow). f, g) Ballen aggregate of quartz (qtz) with relatively homogeneous extinction of ballen (type III) and cristobalite (crs, type I). Image (f) taken with crossed polarizers and compensator plate inserted, sample CT917, compare Fig. 6. h) Quartz aggregate with ballen surrounded by brownish rim of cristobalite in contact with vesicle (vs, type IV, compare Figs. 6, 8a, 8b, 9c and 9d). (Color figure can be viewed at wileyonlinelibrary.com.)

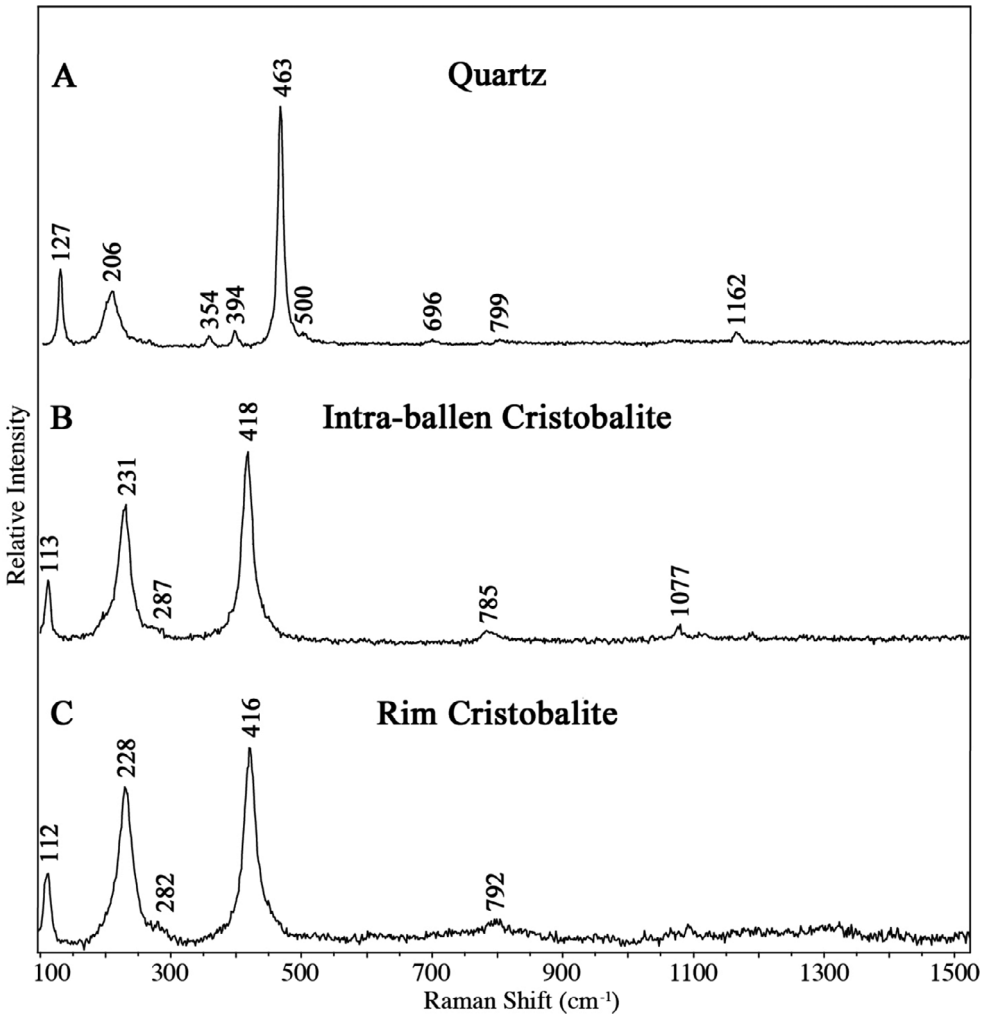

Fig. 3. Raman spectra of (A) α-quartz and (B) α-cristobalite aggregates with ballen (compare Figs. 2d and 2e, respectively). In (C), the Raman spectra of α-cristobalite at the rim surrounding ballen aggregates in contact with vesicles are shown (compare Fig. 2f).

In Table 1, the classification of ballen quartz and cristobalite aggregates after Ferrière et al. (2009), using their extinction characteristics in polarized light, is applied to our observations. The classification is, however, not always explicitly applicable to our samples, as single aggregates commonly show different extinction characteristics in polarized light. Most ballen aggregates (67%) can be classified as type IV, as they show undulatory extinction of individual ballen (Figs. 2c–f and 4a,b). However, 20% of the quartz ballen aggregates show coarser domains of similar extinction, although individual ballen show undulatory extinction (Fig. 2d). About 32% show a "chert-like" extinction characteristic of type V (Fig. 2e), where individual ballen show on small-scale largely different extinction positions. However, ballen aggregates with "chert-like" extinction (type V) can in other parts show rather a heterogeneous type IV extinction (Figs. 2e and 5). Also, ballen aggregates occur that comprise quartz and cristobalite (Figs. 2f and 2g). The cristobalite part of the ballen aggregate would classify as type I with low birefringence; the part comprised by quartz would classify as type III, as it shows relatively homogenous extinction of individual ballen (Fig. 2f). We did not find a systematic difference in the occurrence of the various types within the samples, whether the ballen aggregates are in the center of a granitic gneiss clast, at the rim to the matrix, or within the matrix of the impact melt rock. Yet, in 2-D thin sections, the 3-D distributions of the ballen aggregates within the very heterogeneous impact melt rock are not apparent. To further characterize the ballen aggregates by their crystallographic orientation characteristics, we performed EBSD measurements.

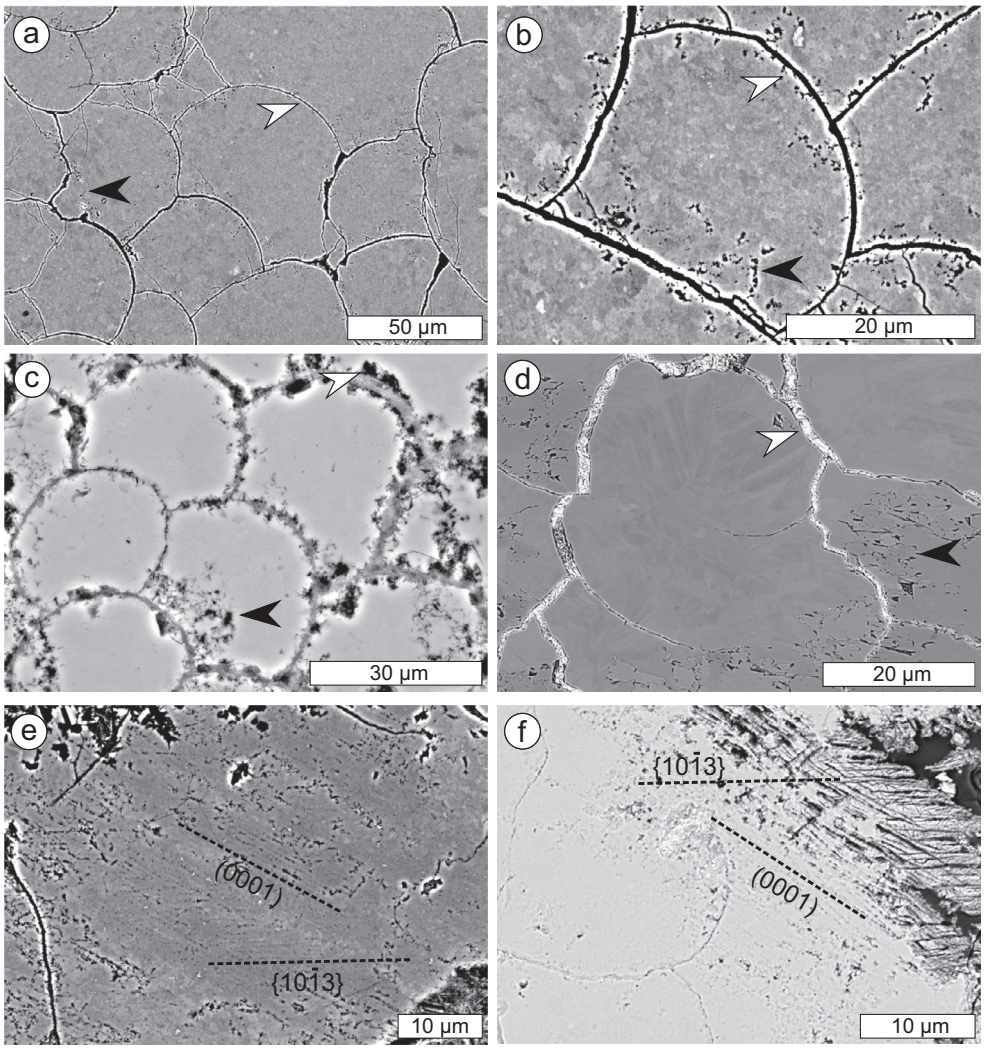

Fig. 4. BSE images of silica aggregates with ballen. a, b) Curved interfaces (white arrows) define the quartz ballen. Note porosity close to the fractures (black arrows) and mottled orientation contrast, sample CT915. c) Siliceous material rich in Fe, K, Al, and Mg decorate fractures (white arrows), sample CT917. d) Cristobalite with radial orientation contrast and siliceous material rich in Si, Fe, K, Al, and Mg along the curved fractures, sample CT917. e, f) Quartz with sets of planes following the basal and the {10-13} rhombohedral planes and ballen aggregate that retains its original shape from the host rock, sample CT917, compare Fig. 2b.

The EBSD measurements reveal that the individual quartz ballen are generally themselves polycrystalline (Figs. 5 and 6a, 6b), consistent with the presence of high-angle grain boundaries (misorientation angle >10°, red lines in Fig. 5c). Low-angle grain boundaries (misorientation angle <10°, yellow lines in Fig. 5c) are relatively rare (Figs. 5c and 6b). The quartz ballen aggregates that classify as types IV and V show a crystallographic preferred orientation (CPO) with one or two dominating orientations, as indicated by EBSD measurements (Figs. 5d, 5f, 5i and 6b, 6c), which is consistent with the optical appearance of similar extinction positions of larger domains (Fig. 2d). These domains are characterized by one marked maximum at low misorientation angles, yet one maximum at about 60° (Fig. 5i), which shows that they contain Dauphiné twin orientations, as also evident from the pole figures (Fig. 5f). Dauphiné twin orientations are characterized by a 60° misorientation angle and a rotation axis parallel to the quartz <c> axis, that is, they do not contribute to a difference in optical extinction. Apart from these dominant orientations characterized by a marked CPO, quartz occurs also in scattered orientations (Figs. 5e and 5g) with an almost random misorientation angle distribution (Fig. 5h).

In a ballen aggregate that comprises cristobalite and quartz (Figs. 2f, 2g and 7), the individual quartz ballen

Table 1. Classification of observed ballen aggregates.

Type according to Ferrière et al. (2009)	Mineral phase	Extinction characteristics in polarized light, crossed polarizers	Textural characteristics		Example shown in Fig.	% in Polsingen samples
			of aggregate	of ballen		
Type I	α-cristobalite	Low birefringence	Almost random	Polycrystalline	2f, 2g, 7	1
Type II	α-quartz	Homogeneous extinction of all ballen in aggregate	–	–	–	–
Type III	α-quartz	Heterogeneous extinction of aggregate but each ballen has relative homogeneous extinction	No CPO	Polycrystalline	2f, 2g, 7	1
Type IV	α-quartz	Heterogeneous extinction of individual ballen	CPO	Polycrystalline	2c, 2e	46
		Homogeneous extinction of domains, individual ballen show heterogeneous extinction			2d, 2f, 6, 9	20
Type V	α-quartz	Chert-like heterogeneous extinction, individual ballen are hardly detectable	CPO	Polycrystalline	2e, 5	32

show a relative homogeneous extinction compared to other observed ballen. EBSD measurements reveal random crystallographic orientations, that is, no CPO (Figs. 7a–c). The cristobalite ballen are polycrystalline with radiating elongate grains (Fig. 4d). The <c> axis orientations are largely scattering but preferentially radiating likewise and the <010> axis is clustered in a point maximum parallel to the normal to the thin section plane (Fig. 7d). The cristobalite found exclusively along the rim of the ballen aggregates (Figs. 2h and 6a, 6b) shows the same texture (compare Figs. 6d and 7d). The shape of the cristobalite grains is dendritic with the long axes of the dendrites radiating outward (Figs. 8a and 8b). The dendritic cristobalite rim shows a high porosity at the direct contact with the ballen aggregate, which is decreasing toward the outer boundary to the matrix (dark area in Figs. 8a and 8b). Barium and sulfur have been detected by EDS to be present at the cristobalite–quartz contact, suggesting the presence of barium sulfate (black arrow, Fig. 8a). More rarely, prismatic cristobalite can occur surrounding the ballen aggregates together with K-feldspar forming the contact with the polyphase matrix of the impact melt rock (Figs. 8c–f and 9c, 9d). Cristobalite in the ballen aggregates as well as cristobalite at the rim and in the matrix is generally enriched in Na_2O (0.4–0.7 wt%) and Al_2O_3 (1.4–1.7 wt%) summing up to about 2 wt%, as indicated from EDS measurements from five different ballen aggregates.

Coarse quartz grains in granitic gneisses of shock stage 0 (Fig. 9a) show typically abundant fluid inclusion trails. In contrast, the quartz ballen aggregates even with only incipient ballen and preserving the original grain shape systematically do not show fluid inclusion trails (Figs. 9b–d).

DISCUSSION

Transition of Quartz to Shock-Induced Amorphous Phase

Bischoff and Stöffler (1984) suggested that different extinction properties of ballen aggregates are characteristic for different shock pressure conditions. Ferrière et al. (2009), however, argued that different types of ballen do not indicate specific shock pressures, as they result from transformations from either shock-induced diaplectic glass or silica melt (lechatelierite). Our observations of different extinction characteristics in polarized light occurring on thin section scale and even within single ballen aggregates confirm that the different types of ballen cannot be taken to indicate specific shock pressures on sample scale. The stress–temperature conditions may vary locally on grain scale or below, given the different response of the polycrystalline and polyphase granitic gneisses to shock loading and unloading. The EBSD measurements show that the ballen types IV and V differentiated by Ferrière et al. (2009, 2010) are characterized by polycrystalline quartz with a varying amount of grains in random orientations relative to dominant orientations resulting in the observed CPO (Figs. 5 and 6). Only in aggregates comprised by both cristobalite and quartz, no CPO is observed (type I/III, Fig. 7). The dominant orientation is interpreted to be inherited from the original quartz grain in the granitic gneiss protolith, opposed to the random orientations, which are interpreted as "new" orientations.

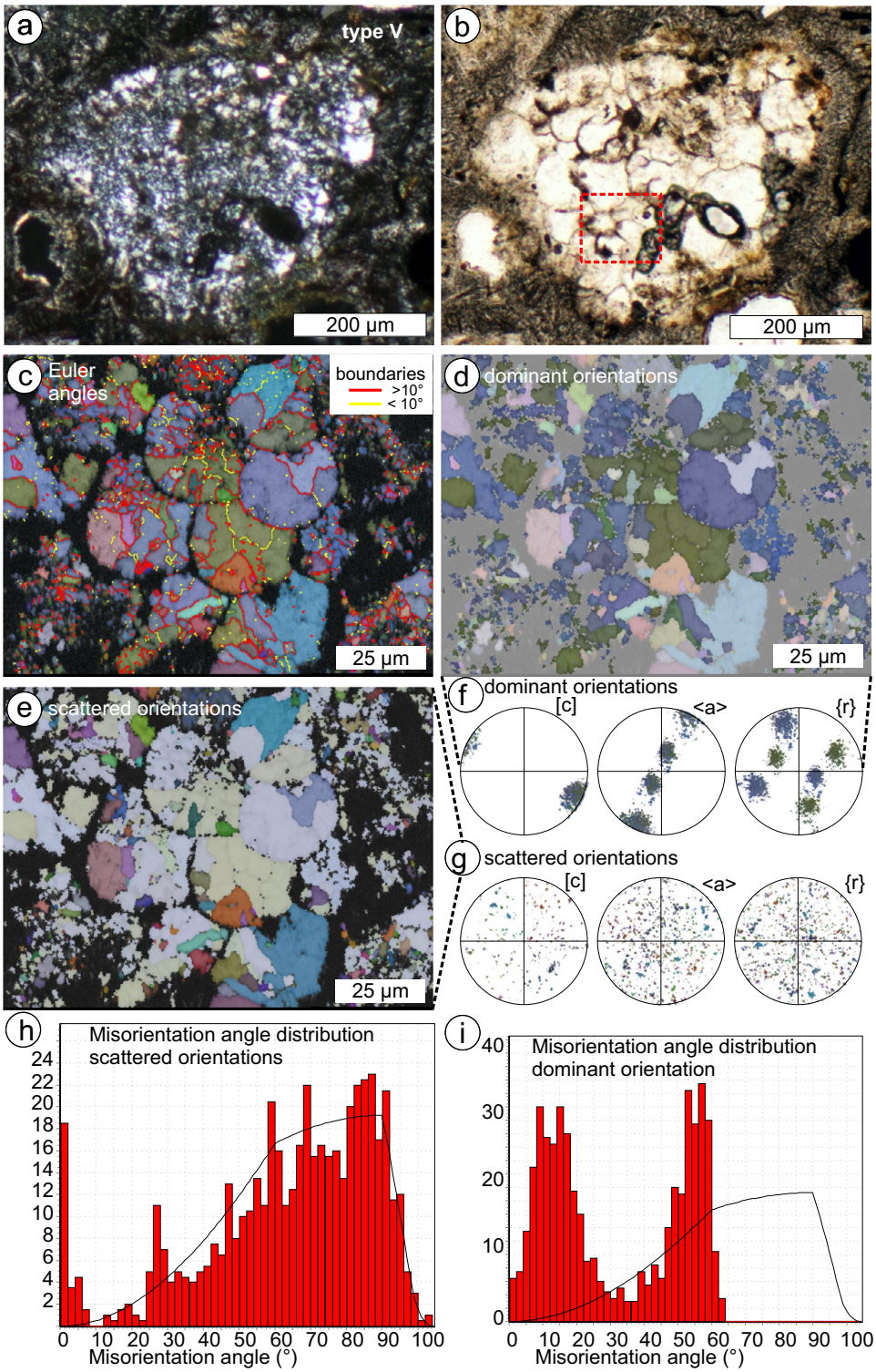

Fig. 5. EBSD data of ballen quartz with "chert-like" extinction (type V), sample CT917. a, b) Polarized light micrographs with and without crossed polarizers, respectively. The red box in (b) indicates the location of the EBSD map. c) Euler angle map overlain by band contrast with boundaries characterized by misorientation angles below (yellow) and above (red) 10°. d, e) Euler angle maps overlain by band contrast, where dominant crystallographic orientation and scattered orientations are highlighted, respectively. f, g) Pole figures of [c], <a>, and {r} axes in stereographic projections of the lower hemisphere, corresponding to the maps in (d) and (e), respectively. h, i) Misorientation angle histograms of scattered, and dominant orientations, corresponding to maps in (d) and (e), respectively.

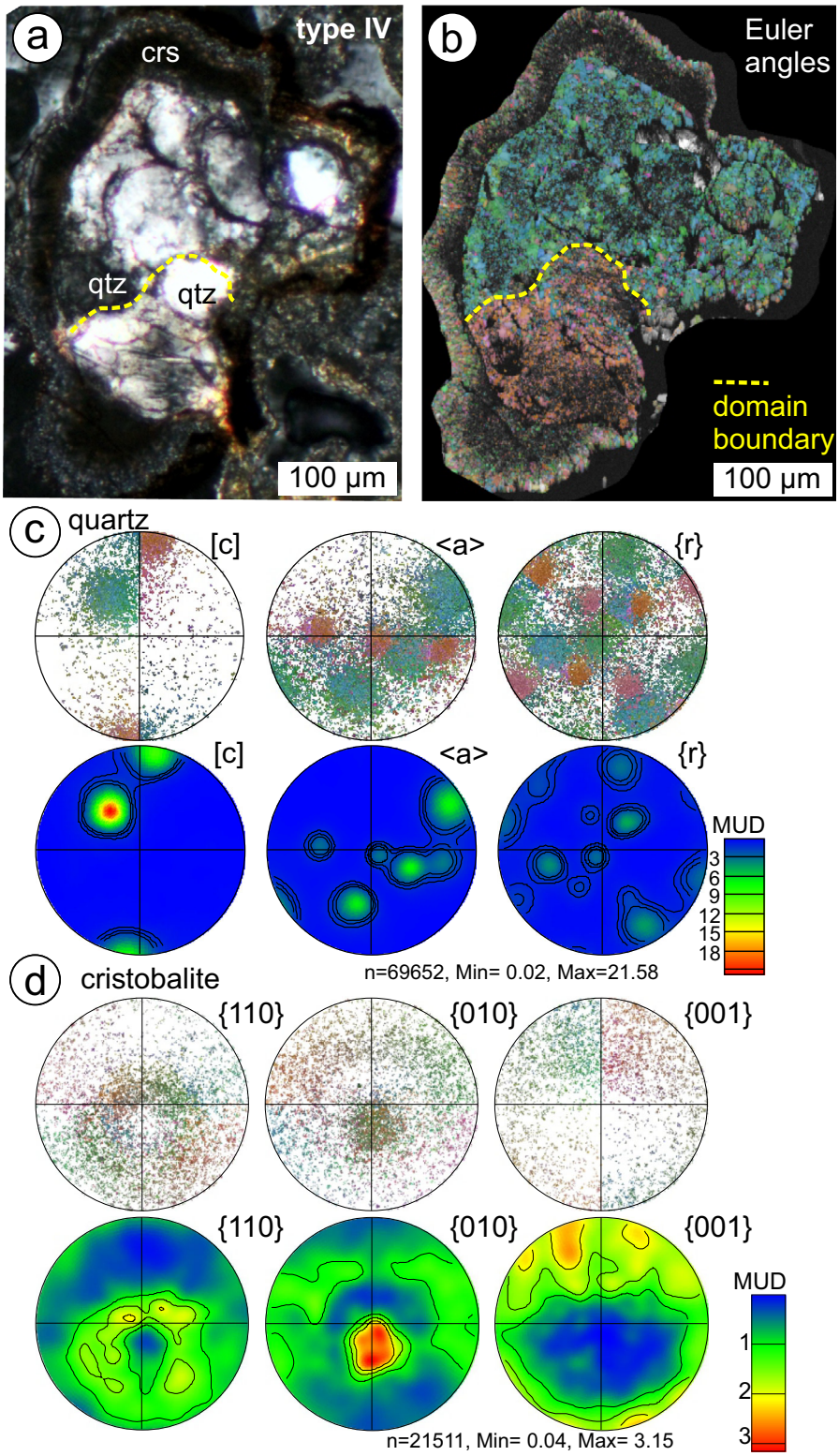

Fig. 6. EBSD data of ballen quartz showing different domains with homogeneous extinction, single ballen show heterogeneous extinction (type IV) and rim of cristobalite, sample CT915 (compare Figs. 2f, h and 7a, b). a, b) Polarized light micrograph (crossed polarizers) and Euler angle map overlain by band contrast, respectively. c) Pole figures of quartz [c], <a>, and {r} axes in stereographic projections of the lower hemisphere, corresponding to the maps in (b). d) Pole figures for cristobalite and density plots in stereographic projections of the lower hemisphere, corresponding to the maps in (b), respectively.

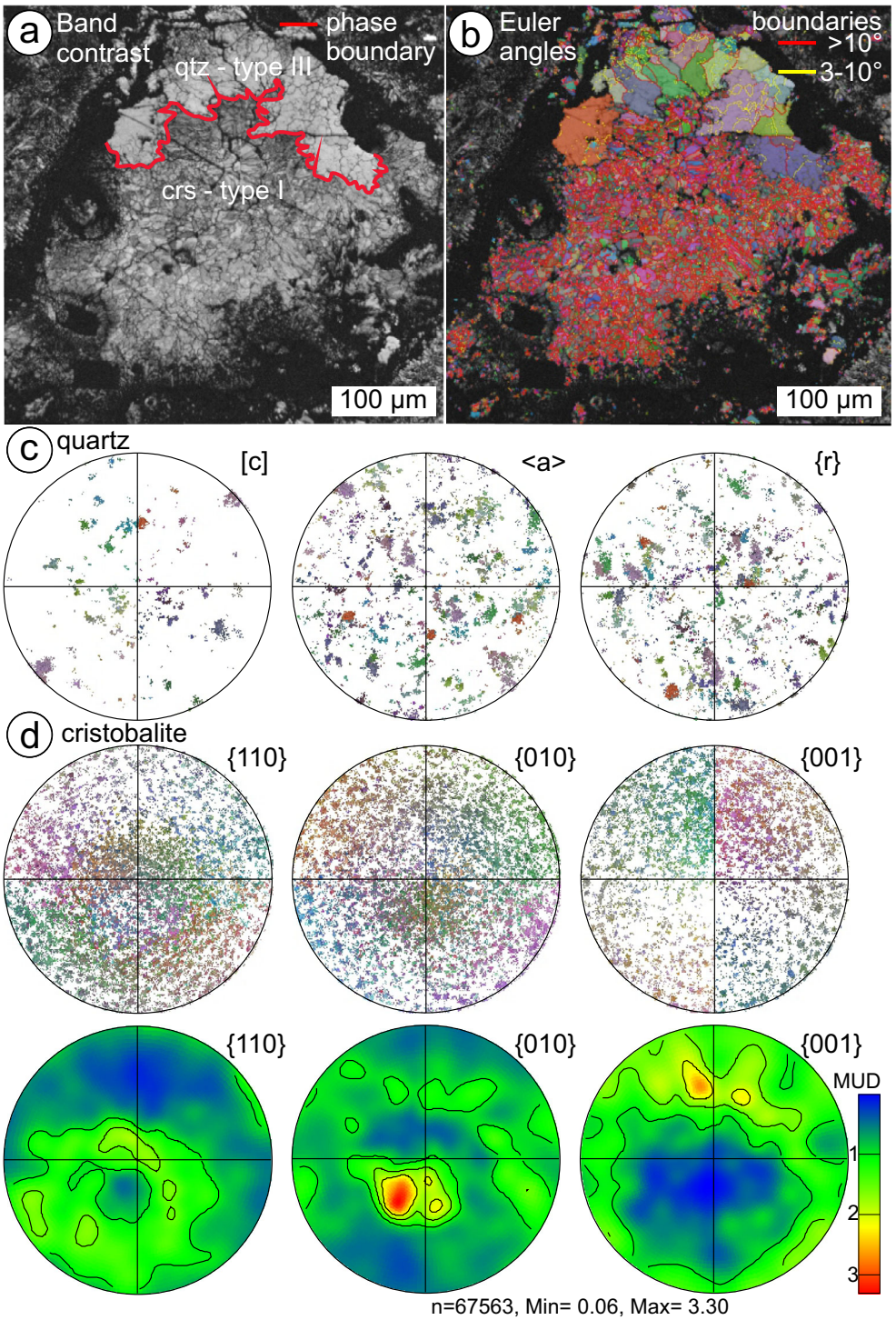

Fig. 7. EBSD data of quartz and cristobalite with ballen, sample CT917 (compare Figs. 2f, 2g). a, b) Band contrast maps with phase boundary between quartz and cristobalite (red line) and map color coded by Euler angles and grain boundaries, respectively. c) Pole figures of quartz [c], <a>, and {r} axes in stereographic projections of the lower hemisphere, corresponding to the maps in (b). d) Pole figures for cristobalite and density plots in stereographic projections of the lower hemisphere, corresponding to the maps in (b), respectively.

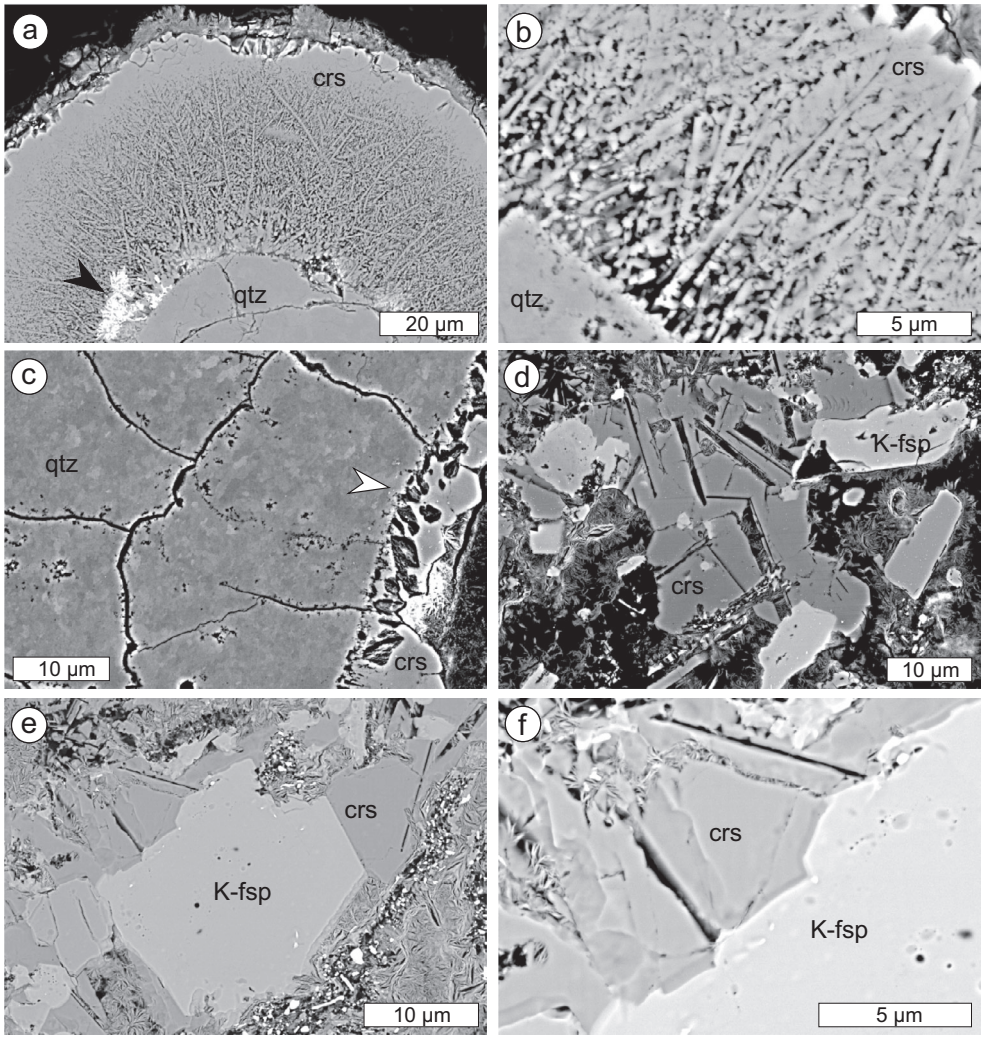

Fig. 8. BSE images of cristobalite microstructures at the rim of ballen aggregates. a, b) Dendritic structure of rim around quartz aggregate with ballen, sample CT915 (compare Fig. 2h and Fig. 6). c) Cristobalite grains at rim of quartz aggregated with ballen, sample CT915. d–f) Cristobalite grains next to K-feldspar at the rim of quartz with incipient ballen, sample CT917 (compare Fig. 2b, Figs. 9b–d). (Color figure can be viewed at wileyonlinelibrary.com.)

We take the observed CPO as a strong indication that the original quartz grains were transformed upon shock loading and rapid unloading into a heterogeneous amorphous phase with varying degree of distortion of the original crystallographic precursor structure. The interpretation, that a transformation from primary quartz from the target rock to a rapidly quenched/decompressed silica melt or diaplectic silica glass is the initial formation mechanism of ballen, is widely accepted (e.g., Carstens 1975; Ferrière et al. 2009, 2010; Buchner et al. 2010). Diaplectic glass is a dense amorphous phase formed during shock compression (e.g., Engelhardt et al. 1967; Hörz and Quaide 1973; Arndt et al. 1982; Kruger and Jeanloz 1990; Langenhorst 1994). Characteristic for diaplectic glass is a preserved short-range order of the precursor structure due to rapid decompression and cooling, such that the glass retains remnants of the original shape and crystal structure. Arndt et al. (1982) suggested that due to the short duration of the shock-induced transient high-temperature excursions, the crystal to melt transition does not come to completion, resulting in a diaplectic glass as disordered transitional state intermediate between the structures of the crystalline and quenched molten phase. As such, any difference between a diaplectic glass without transition to a melt on the one hand and a glass generated from rapidly quenched shock-induced melt on the other hand might not be sharp but rather be of a gradual nature. Diaplectic glass can be expected to be of heterogeneous structure, with variable degrees of the precursor structure

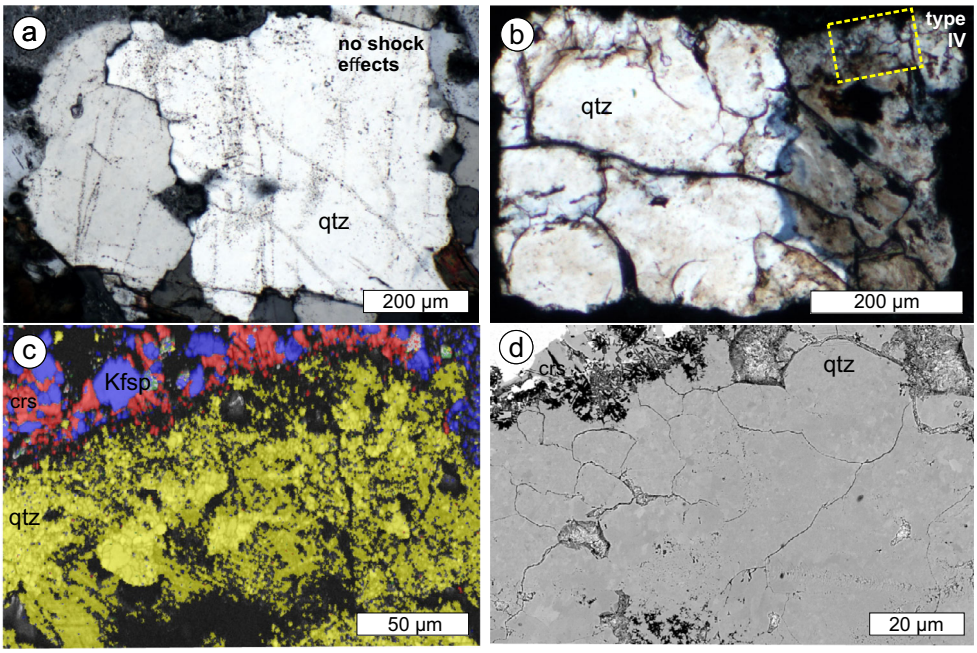

Fig. 9. a) Polarized light micrographs with crossed polarizers showing quartz grain with typical abundant fluid inclusion trails from granitic gneisses, shock stage 0, sample CT830 (Maihingen). b) Polarized light micrographs with crossed polarizers showing polycrystalline quartz aggregate with incipient ballen (type IV), with the shape of the original single crystal preserved sample CT917 (compare Fig. 2b). Yellow rectangle shows location of EBSD map in (c) and BSE image in (d). c) EBSD phase map showing polycrystalline quartz with ballen (yellow), K-feldspar (blue), and cristobalite (red) at the rim. d) BSE image of the same area shown in (c).

being present. Whereas quartz crystallizing from diaplectic silica is found to rather form polycrystalline aggregates (e.g., Rehfeldt-Oskierski et al. 1986; Trepmann 2008), feldspar is typically back-transforming as single crystal with only minor misorientations (e.g., Arndt et al. 1982).

The textural characteristics of the quartz ballen aggregates with CPO together with various amounts of new random orientations (Figs. 5 and 6a–c) are consistent with crystallization of quartz from a diaplectic glass and/or from a rapidly quenched highly viscous, supercooled silica melt, that is, a heterogeneous disordered quenched transition state intermediate between the structure of the crystalline and quenched molten phase. Topotactic crystallization of the diaplectic glass with preserved short range order of the precursor structure leads to the dominating orientation of quartz, whereas crystallization from the more strongly disordered amorphous phase leads to crystallization of quartz with random orientation.

The observed shape of the aggregates is irregular ranging from rectangular (Fig. 2b) to a droplet shape (Fig. 2c), indicating variable degrees of modification from the precursor quartz grain. Independent of their shape, most observed ballen aggregates show a CPO (Table 1). Even in the case of the mixed quartz and cristobalite ballen, the shape of the aggregate is rather rectangular (Figs. 2f and 2g). Given the textural and structural characteristics, we suggest that the ballen aggregates are derived from coarse quartz grains of the granitic gneiss protolith that were transformed to an amorphous silica phase with various amounts of information on the precursor structure upon shock loading and rapid unloading.

Role of Multiple Phase Transformations

To explain the specific microstructure of ballen and the related occurrence of cristobalite, further multiple transformations mostly from cristobalite to quartz have been suggested (e.g., Engelhardt 1972; Carstens 1975; Ferrière et al. 2009, 2010; Buchner et al. 2010). Ferrière et al. (2010) came to the conclusion that α-quartz ballen are the result of back-transformation from either α-cristobalite or β-quartz with time. For our samples, a phase transformation from β-quartz originally crystallized from the shock-induced amorphous phase to α-quartz might be indeed suggested by the occurrence of Dauphiné twin orientations (Fig. 5), as reported, for example, also for shocked quartz from the Charlevoix structure (Trepmann and Spray 2005). Yet, the displacive α-quartz to β-quartz phase transition cannot explain the globular shape of the ballen. Ferrière et al.

(2009) discussed that the volume change from cristobalite to quartz is responsible for the different types of ballen silica (types II, III, IV, V). Yet, as also cristobalite ballen occur, the cristobalite to quartz phase transition cannot be a prerequisite for the globular shape. Furthermore, our observations do not provide any evidence for a cristobalite to quartz transition. In contrast, the commonly observed CPO interpreted as inherited from the precursor quartz suggests direct crystallization of quartz (either α- or β-quartz) from a diaplectic glass. The phase transition from the topology of the cristobalite structure (tetragonal α- or cubic β-cristobalite) to the topology of the quartz structure (hexagonal β- or trigonal α-quartz) would require the complete restructuring of the tetrahedral network, which is incompatible with the observed CPO for symmetry reasons. Likewise, the rarely observed sets of planar features parallel to crystallographic planes in ballen quartz (Figs. 4e and 4f) would be difficult to explain by multiple phase transformations (from quartz to an amorphous phase to cristobalite and back to quartz), as already discussed by other authors (e.g., Buchner et al. 2010; Chanou et al. 2015).

Formation of Ballen Shape—Dehydration of Amorphous Phase

The ballen resembles perlitic structures, that is, globular microstructures, known from cristobalite in silica-rich andesitic to rhyolitic volcanic rocks and hydrated glass (obsidian, e.g., Swanson et al. 1989; Horwell et al. 2013). On the basis of experimental evidence, Marakushev et al. (1988) interpreted perlitic structures to form due to the solidification of hydrous silica-rich melts with hindered dehydration. Due to the separation of the water phase during decompression and cooling, strain concentrations cause peeling and radial cracks in the crystallizing glass (Marakushev et al. 1988). In andesitic–rhyolitic volcanic rocks, cristobalite commonly occurs in pores and fractures as a precipitate from a vapor phase or by devitrification from an amorphous volcanic glass. K-feldspar can be associated within spherulites in devitrified obsidian domes and rhyolitic lavas (e.g., Swanson et al. 1989; Horwell et al. 2013). The cristobalite stability field ranges between 1470 and 1713 °C at <1 GPa, but cristobalite can exist as a metastable phase due to the required activation energy for the reconstructive transformation of cristobalite to low quartz. Cristobalite can grow in dendritic to spherulitic deposits on a cold (200–700 °C) quartz substratum from hydrothermal fluids at high temperature gradients (100–600 °C) as demonstrated in the experiments by Flörke et al. (1990).

We suggest the following: The original quartz crystals from granitic gneisses in the Ries contain abundant fluid inclusions (Fig. 9a). Upon shock loading, the fluid inclusion-rich quartz grains transformed into an amorphous silica phase, in which the volatiles dissolved. During decompression and cooling, the amorphous silica phase dehydrates and a water-rich fluid is generated, which results in strain concentrations causing radial "dehydration cracks," comparable to the perlitic structure in volcanic rocks (Marakushev et al. 1988). Such dehydration is consistent with the common observation of an increased porosity close to the curved interface between the ballen (black arrow in Fig. 4b). The water-rich fluid is expelled along the curved dehydration cracks. Water contents in fluid inclusion-rich quartz in granitoid rocks is typically on the order of 7000–14,000H/10^6 Si (approximately 0.1–0.2 wt% H_2O; Kronenberg and Wolf 1990; Kilian et al. 2016). This water content is close to what is required for the formation of perlitic structures in obsidians (H_2O contents 0.1–4.8 wt%; Marakushev et al. 1988).

Dendritic cristobalite is exclusively observed at the outer rim of the ballen aggregates in contact with vesicles (Figs. 2h, 5a, 5b, 6a). Its occurrence is therefore interpreted to be related to the ballen formation. Cristobalite probably crystallized directly from the volatile-rich melt that was expelled from the amorphous silica phase, possibly involving degassing to form the vesicles, as also suggested for volcanic perlites (e.g., Horwell et al. 2013). If associated with K-feldspar, some prismatic cristobalite can surround the ballen aggregates. These fine-grained polyphase aggregates are likewise interpreted to have crystallized directly from a silica-rich melt (Figs. 8d–f and 9c, 9d).

Cristobalite occurring as radiating elongate crystals within the ballen aggregates together with quartz without CPO (Fig. 7) is suggested to have crystallized from a rapidly quenched highly viscous, supercooled silica amorphous phase with no memory of the precursor phase, as opposed to quartz ballen with CPO. In this sense, the specific microstructures are suggested to reflect a different degree of disordering of the shock-induced amorphous phase from which they formed. (1) Ballen quartz with sets of planar features parallel to crystallographic planes of the precursory quartz grain is indicative of a shocked SiO_2 material, which still retains significant crystalline order; (2) ballen quartz with CPO crystallized from amorphous silica with remnants of crystalline long-range order to dominate nucleation; (3) ballen quartz with random texture crystallized from an amorphous silica, where the long-range order of quartz was totally destroyed; and (4) cristobalite occurs if the quartz-like short-range order is completely lost and/or if contamination of the silica by components like

Na^{+} and Al^{3+} has occurred. These different microstructures are interpreted to reflect locally heterogeneous stress–temperature conditions on grain scale or below, due to the different response of the polycrystalline and polyphase granitic gneisses to shock loading and unloading (i.e., differences in crystallographic orientation, structure, phase, shape, fluid content, etc.).

We would like to point out that planar deformation features in quartz are known as shock compression-induced incomplete transformation into diaplectic silica glass localized along crystallographic planes (e.g., Goltrant et al. 1992a, 1992b; Langenhorst 1994). The commonly observed fluid inclusions present along annealed planar deformation features in shocked quartz (e.g., Goltrant et al. 1992a, 1992b; Leroux and Doukhan 1996; Trepmann and Spray 2006; Trepmann 2008) would be consistent with our interpretation of the dissolution of volatiles initially present in fluid inclusions from the precursory quartz grains into diaplectic glass upon shock loading and dissolving of the fluid upon decompression and cooling. Upon shock compression, the water in the crystal segregates locally along specific crystallographically controlled planes and dissolves into the generated diaplectic glass. Upon decompression and cooling, water is expelled again as fluid inclusions that are observable along annealed PDFs.

CONCLUSIONS

Based on our observations on Ries impact melt rocks, we come to the following conclusions:

1. The observed ballen aggregates are derived from coarse original quartz grains from the granitic gneiss protolith. Upon shock loading, quartz is transformed to a diaplectic glass and/or a highly viscous, supercooled silica melt.
2. Topotactic crystallization of the diaplectic glass with preserved short range order of the precursor structure leads to dominant crystallographic orientations, whereas crystallization from the more strongly disordered amorphous phase leads to crystallization of quartz with random orientation.
3. Cristobalite within ballen aggregates crystallized from a shock-induced amorphous phase with no memory of the precursor phase remaining.
4. From the microstructural and textural observations in our samples, there is no indication for a phase transformation from cristobalite to quartz.
5. We suggest that the globular shape of ballen in our samples is due to dehydration and associated cracking during rapid decompression and cooling of the amorphous phase, similar to perlitic structures in volcanic rocks.
6. Cristobalite, quartz with random texture, quartz with CPO, and quartz with remnants of crystallographically controlled planar features present in ballen aggregates are interpreted to represent a decreasing degree of disordering of the amorphous phase originating from shock compression of the precursor quartz grains.
7. In contrast, dendritic cristobalite occurring at the rim of quartz ballen aggregates in contact with vesicles crystallized directly from a melt enriched in fluids that were expelled from the dehydrating glass and/or melt.

Acknowledgments—The thoughtful and constructive reviews of Fred Hörz and Ludovic Ferrière as well as the editorial handling by Christian Koeberl are greatly appreciated. We gratefully acknowledge funding from the *Staatliche naturwissenschaftliche Sammlungen Bayerns* (SNSB-Innovativ). Namvar Jahanmehr and Corrina Franke are acknowledged for thin section preparation and assistance with polarized light microscopy, respectively. Open access funding enabled and organized by Projekt DEAL.

Editorial Handling—Dr. Christian Koeberl

REFERENCES

Arndt J., Hummel W., and Gonzalez-Cabeza I. 1982. Diaplectic labradorite glass from the Manicouagan impact crater—I. Physical properties, crystallization, structural and genetic implications. *Physics and Chemistry of Minerals* 8:230–239.

Bischoff A. and Stöffler D. 1984. Chemical and structural changes induced by thermal annealing of shocked feldspar inclusions in impact melt rocks from Lappajärvi crater, Finland. *Journal of Geophysical Research* 89:B645–B656.

Boyer H., Smith D. C., Chopin C., and Lasnier B. 1985. Raman microprobe (RMP) determinations of natural and synthetic coesite. *Physics and Chemistry of Minerals* 12:45–48.

Buchner E., Schwarz W. H., Schmieder M., and Trieloff M. 2010. Establishing a 14.6 ± 0.2 Ma age for the Nördlinger Ries impact (Germany)—A prime example for concordant isotopic ages from various dating materials. *Meteoritics & Planetary Science* 45:662–674.

Carstens H. 1975. Thermal history of impact melt rocks in the Fennoscandian shield. *Contributions to Mineralogy and Petrology* 50:145–155.

Chanou A., Grieve R. A. F., and Osinski G. R. 2015. Formation of ballen in silica by thermal shock (abstract). In *Bridging the gap III Conference*, University of Freiburg, Conference, organized by Kenkmann T., Poelchau M.H., Deutsch A. University of Freiburg, Freiburg. Germany. pp. 12–13.

Chen M., Xiao W., and Xie X. 2010. Coesite and quartz characteristic of crystallization from shock-produced silica melt in the Xiuyan crater. *Earth and Planetary Science Letters* 297:306–314.

Engelhardt W. von. 1972. Shock produced rock glasses from the Ries crater. *Contributions to Mineralogy and Petrology* 36:265–292.

Engelhardt W. von, and Graup G. 1984. Suevite of the Ries crater, Germany: Source rocks and implications for cratering mechanics. *Geologische Rundschau* 73:447–481.

Engelhardt W. von. 1997. Suevite breccia of the Ries impact crater, Germany: Petrography, chemistry and shock metamorphism of crystalline rock clasts. *Meteoritics & Planetary Science* 32:545–554.

Engelhardt W. von. Arndt J., Stöffler D., Müller W. F., Jeziorkowski H., and Gubser R. A. 1967. Diaplektische Gläser in den Breccien des Ries von Nördlingen als Anzeichen für Stoßwellenmetamorphose. *Contributions to Mineralogy and Petrology* 15:93–102.

Ferrière L., Koeberl C., Reimold W. U., Libowitzky E., and Greshake A. 2008. Ballen quartz and cristobalite in impact breccias: Types, occurrence, and possible origin (abstract #3011). Large Meteorite Impacts and Planetary Evolution IV. Vredefort Dome, South Africa. pp. 3–4.

Ferrière L., Koeberl C., and Reimold W. U. 2009. Characterisation of ballen quartz and cristobalite in impact breccias: New observations and constraints on ballen formation. *European Journal of Mineralogy* 21:203–217.

Ferrière L., Koeberl C., Libowitzky E., Reimold W. U., Greshake A., and Brandstätter F. 2010. Ballen quartz and cristobalite in impactites: New investigations. In *Large meteorite impacts and planetary evolution IV*, edited by Gibson R. L. and Reimold W. U. *Geological Society of America Special Paper* 465:609–618.

Flörke O., Graetsch H., and Jones J. 1990. Hydrothermal deposition of cristobalite. *Neues Jahrbuch für Mineralogie Monatshefte*. 2:81–95.

French B. M. 1998. *Traces of catastrophe: A handbook of shock-metamorphic effects in terrestrial meteorite impact structures*. Houston, Texas: Lunar and Planetary Institute. 120 p.

Goltrant O., Leroux H., Doukhan J. C., and Cordier P. 1992a. Formation mechanisms of planar deformation features in naturally shocked quartz. *Physics of the Earth and Planetary Interiors* 74:219–240.

Goltrant O., Doukhan J.-C, Cordier P., and Courtillot V. 1992b. An investigation by transmission electron microscopy of planar deformation features in naturally shocked quartz. *Terra Nova* 4:405–412.

Horwell C. J., Williamson B. J., Llewellin E. W., Damby D. E., and Le Blond J. S. 2013. The nature and formation of cristobalite at the Soufrière Hills volcano, Montserrat: Implications for the petrology and stability of silicic lava domes. *Bulletin of Volcanology* 75:1–19.

Hörz F. and Quaide W. L. 1973. Debye-Scherrer investigations of experimentally shocked silicates. *The Moon* 6:45–82.

Kilian R., Heilbronner R., Holyoke C.W.I., Kronenberg A. K., and Stunitz H. 2016. Dislocation creep of dry quartz. *Journal of Geophysical Research: Solid Earth* 121:3278–3299.

Kronenberg A. and Wolf G. 1990. Fourier transform infrared spectroscopy determinations of intragranular water content in quartz-bearing rocks: Implications for hydrolytic weakening in the laboratory and within the Earth. *Tectonophysics* 172(3–4):255–271.

Kruger M. B. and Jeanloz R. 1990. Memory glass: An amorphous material formed from $AlPO_4$. *Science* 249:647–649.

Langenhorst F. 1994. Shock experiments on pre-heated α- & β-quartz: II. X-ray and TEM investigations. *Earth and Planetary Science Letters* 128:683–698.

Leroux H. and Doukhan J.-C. 1996. A transmission electron microscope study of shocked quartz from the Manson impact structure. In *The Manson impact structure, Iowa: Anatomy of an impact crater*, edited by Koeberl C. and Anderson R. R. *Geological Society of America Special Paper* 302:267–274.

Marakushev A. A., Persikov E. S., and Bukhtiarov P. G. 1988. Endogenic nature of perlites. In *2nd International Conference on Natural Glasses*, edited by Konta J. Prague, Czech Republic: Charles University. pp. 89–96.

Osinski G. R. 2004. Impact melt rocks from the Ries structure, Germany: An origin as impact melt flows? *Earth and Planetary Science Letters* 226:529–543.

Rehfeldt-Oskierski A., Stöffler D., and Hornemann U. 1986. Deformation, transformation, and thermal annealing of experimentally shocked single crystal quartz (abstract). 17th Lunar and Planetary Science Conference. pp. 697–698.

Schmieder M., Jourdan F., Tohver E., and Cloutis E. A. 2014. $^{40}Ar/^{39}Ar$ age of the Lake Saint Martin impact structure (Canada)—Unchaining the Late Triassic terrestrial impact craters. *Earth and Planetary Science Letters* 406:37–48.

Short N. M. 1970. Progressive shock metamorphism of quartzite ejecta from the Sedan nuclear explosion crater. *The Journal of Geology* 78:705–732.

Stähle V., Altherr R., Koch M., and Nasdala L. 2008. Shock-induced growth and metastability of stishovite and coesite in lithic clasts from suevite of the Ries impact crater (Germany). *Contributions to Mineralogy and Petrology* 155:457–472.

Stöffler D., Artemieva N. A., Wünnemann K., Reimold W. U., Jacob J., Hansen B. K., and Summerson I. A. T. 2013. Ries crater and suevite revisited—Observations and modeling Part I: Observations. *Meteoritics & Planetary Science* 48:515–589.

Stöffler D., Hamann C., and Metzler K. 2018. Shock metamorphism of planetary silicate rocks and sediments proposal for an updated classification system. *Meteoritics & Planetary Science* 53:5–49.

Swanson S. E., Naney M. T., Westrich H. R., and Eichelberger J. C. 1989. Crystallization history of Obsidian Dome, Inyo Domes, California. *Bulletin of Volcanology* 51:161–176.

Trepmann C. A. 2008. Shock effects in quartz: Compression versus shear deformation—An example from the Rochechouart impact structure, France. *Earth and Planetary Science Letters* 267:322–332.

Trepmann C. A. and Spray J. G. 2005. Planar microstructures and Dauphiné twins in shocked quartz from the Charlevoix impact structure, Canada. In *Large meteorite impacts III*, edited by Kenkmann T., Hörz F., and Deutsch A. *Geological Society of America Special Paper*, 384, 315–328.

Trepmann C. A. and Spray J. G. 2006. Shock-induced crystal-plastic deformation and post-shock annealing of quartz: Microstructural evidence from crystalline target rocks of the Charlevoix impact structure, Canada. *European Journal of Mineralogy* 18:161–173.

Whitehead J., Grieve R. A. F., and Spray J. G. 2002. Mineralogy and petrology of melt rocks from the Popigai impact structure, Siberia. *Meteoritics & Planetary Science* 37:623–647.